INORGANIC CHEMISTRY
FRONTIERS

RESEARCH ARTICLE

View Article Online
View Journal | View Issue



Cite this: *Inorg. Chem. Front.*, 2018, **5**, 1575

# Dramatic impact of the lattice solvent on the dynamic magnetic relaxation of dinuclear dysprosium single-molecule magnets†

Wan-Ying Zhang, [a] Yi-Quan Zhang, [b] Shang-Da Jiang, [c] Wen-Bin Sun, *[a] Hong-Feng Li, [a] Bing-Wu Wang, *[c] Peng Chen, [a] Peng-Fei Yan *[a] and Song Gao *[c]

Received 26th March 2018,
Accepted 28th April 2018

DOI: 10.1039/c8qi00266e

rsc.li/frontiers-inorganic



Two dinuclear dysprosium single-molecule magnets (SMMs) with a nearly identical core structure, namely $[Dy_2(DMOP)_2(DBM)_4(CHCl_3)_4]$ (**1**) and $[Dy_2(DMOP)_2(DBM)_4(C_2H_4Cl_2)_2]$ (**2**) (DMOP = 2,6-dimethoxyphenol, DBM = dibenzoylmethane), and their Y(III) (**3**) and Gd(III) (**4**) analogues were structurally and magnetically characterized. Despite the fact the phenoxyl of DMOP can only transfer weak exchange coupling and the local coordination environment around the individual Dy(III) ion is in a low geometrical symmetry, their joint contribution ultimately leads to significant zero-field slow magnetic relaxation behaviours. It is interesting to note that the effective energy barrier ($U_{eff}$) of the magnetization reversal was nearly doubly improved by only deliberately replacing or losing the lattice solvents while maintaining the Dy2 core structure. *Ab initio* calculations confirmed that changing the lattice solvents induced the intramolecular coupling change and impacted the dynamic magnetic relaxations. The significant enhancement of an SMM's performance depending on the lattice solvents indicated that it is possible to improve an SMM's properties by tuning the guest molecules.

## Introduction

The large magnetic anisotropy of lanthanide(III) ions stem from strong spin–orbit coupling and a crystal field effect that makes 4f-based single-molecule magnets (SMMs) display significant slow magnetic relaxation behaviours with high energy barriers ($U_{eff}$) for the reversal of magnetization and the blocking temperature ($T_B$).[1] Their unique magnetic properties connecting the conventional and quantum world make SMMs good candidates for high-density information storage, quantum information processing, molecular spintronics and magnetic cooling applications.[2] For lanthanide-based SMMs, the magnetic anisotropy mostly arises from the single-ion magnetic anisotropy due to the intrinsic shielded 4f electrons of lanthanide(III) ions.[2e,f] However, the slow magnetic relaxation is normally sensitive to the crystal field and/or ligand field as well as to the local symmetry surrounding the lanthanide(III) ion.[3] This meanwhile provides an opportunity to fine-tune the slow magnetic relaxation through modulating the local symmetry and peripheral ligand field.[4] A few reports have indicated that modulating the local symmetry and ligand field is effective to construct single-ion magnets (SIMs, mononuclear SMMs) with higher $U_{eff}$ and $T_B$;[5] for instance an energy barrier beyond 1000 K in pentagonal bipyramidal Dy(III) SIM,[6] and up to 60 K $T_B$ have been obtained in dysprosium metallocene $[Dy(Cp^{ttt})_2][B(C_6F_5)_4]$ ($Cp^{ttt}$ = 1,2,4-tri(*tert*-butyl)cyclopentadienide).[7] However, such a strategy has a finite ceiling of improvement due to the flexible coordination modes and high coordination numbers of lanthanide(III) ions, which usually result in a low axial coordination symmetry. In addition, the quantum tunnelling of magnetization (QTM), involving a fast relaxation through near-degenerate ground states, prevails in nearly all lanthanide SIMs and has become a serious factor impeding the development of lanthanide SMMs with a better performance. Clearly, considering both the local high axial symmetry and coupled spin is an effective strategy to improve

[a]*Key Laboratory of Functional Inorganic Material Chemistry Ministry of Education, School of Chemistry and Material Science Heilongjiang University, 74 Xuefu Road, Harbin 150080, P. R. China. E-mail: wenbinsun@126.com, yanpf@vip.sina.com*
[b]*Jiangsu Key Laboratory for NSLSCS, School of Physical Science and Technology, Nanjing Normal University, Nanjing 210023, P. R. China. E-mail: zhangyiquan@njnu.edu.cn*
[c]*Beijing National Laboratory of Molecular Science State Key Laboratory of Rare Earth Materials Chemistry and Applications, College of Chemistry and Molecular Engineering, Peking University, Beijing 100871, China. E-mail: wangbw@pku.edu.cn, gaosong@pku.edu.cn*

†Electronic supplementary information (ESI) available: Additional structural, magnetic data and the methods/results for *ab initio* calculation for the complexes. CCDC 1411817, 1411818, 1413255 and 1413256. For ESI and crystallographic data in CIF or other electronic format see DOI: 10.1039/c8qi00266e

the magnetic anisotropy.[8] Appropriate intramolecular couplings have been proven to suppress QTM significantly[9] and have exhibited predominant relaxation properties. High $T_B$ values of 14 K and 12 K were observed in a dinuclear Tb2 system bridged by an $N^{3-}$ radical[10] and an Er2 complex sandwiched by multilayer COT (COT = cyclooctatetraenyl) and substituent COT.[11] The bridging ligands play a crucial role in these systems. The radical approach is a successful way to obtain large laterally exchanged coupling interactions effectively between two lanthanide ions owing to the presence of an unpaired electron on the ligand. Alternatively, in the multilayer sandwich COT-Ln SMMs, the COT ligand could transfer the longitudinally coupling, offering a delocalized superexchange pathway. However, extending this methodology to larger molecules involving multiple metal centres/radicals and multilayer organometallic species is synthetically very difficult.[12] In comparison, neutral organic bridges can transmit magnetic coupling, albeit a little weak, but sufficient to also influence the magnetic state of the ground and even excited state and consequently can change the magnetic relaxation of the whole molecule dramatically.[13] The joint contribution of local symmetry and appropriate intramolecular coupling is highly promising to improve the performance of dinuclear lanthanide-based SMMs. Additionally, recently, a new chemical strategy for the construction of molecular nanomagnets by constraining the coordination symmetries around lanthanide centres within metal–organic frameworks (MOFs) was developed to tune the properties of SMMs.[14] As a novel way to control and modulate the molecular magnetic anisotropy, the impact of guest molecules in MOFs and lattice solvents in crystals on the magnetic relaxation properties has attracted increasing attention,[15] although such effects had already been pointed out before.[16] We recently found that the ligand 2,6-dimethoxyphenol (DMOP) is a good candidate but has barely been used to construct dinuclear SMMs.[17] Interestingly, a dramatic influence of the lattice solvents on the magnetic relaxation was observed, which is a potential factor to improve an SMM's performance. Herein, we report details on the preparations, structures and magnetic properties of two dinuclear dysprosium complexes with different lattice solvents, namely $[Dy_2(DMOP)_2(DBM)_4(CHCl_3)_4]$ (**1**) and $[Dy_2(DMOP)_2(DBM)_4(C_2H_4Cl_2)_2]$ (**2**).

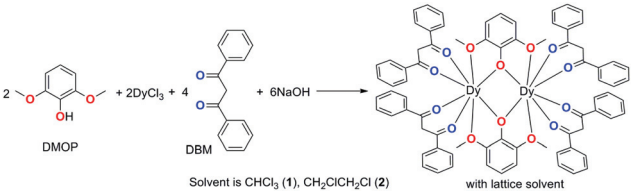


**Scheme 1** Synthesis of complexes **1** and **2**.

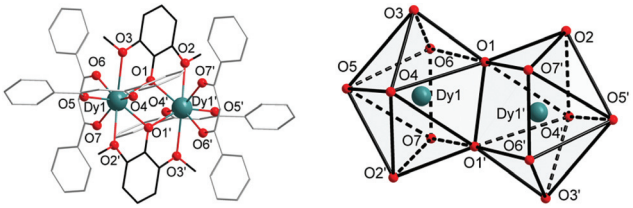


**Fig. 1** Molecular structure of complex **1** with atomic labelling, in which a symmetry code was used to generate equivalent atoms: Dy′ and O′ (left), and the biaugmented trigonal prism of the $[DyO_8]$ cores (right), hydrogen atoms have been omitted for clarity; symmetry codes: Dy1′: 1 − *x*, −*y*, −*z* + 1.

## Results and discussion

### Synthesis and characterization

Complexes **1** and **2** were synthesized as shown in Scheme 1. They were recrystallized from solvents $CHCl_3$ and $CH_2ClCH_2Cl$ as the guest molecule in lattices **1** and **2**, respectively. Complexes **1** and **2** could transform to each other through losing their respective guest molecules and recrystallizing from the opponent solvent. Complex **1** crystallizes in the triclinic space group $P\bar{1}$, with the molecular structure of **1** shown in Fig. 1. The asymmetric unit consists of one Dy(III) ion, one $DMOP^-$ ligand, two $DBM^-$ ligands and two lattice $CHCl_3$ molecules. Each Dy(III) ion is surrounded by eight oxygen atoms belonging to two chelating $DMOP^-$ ligands and two $DBM^-$ ligands. The phenoxy oxygen of each ligand $DMOP^-$ adopts a μ-bridge mode between the two Dy(III) ions (Fig. 1, left). The local symmetry of Dy(III) ion was analyzed using the parameter *S* of the continuous-shape-measures (CShMs) method,[18] which allowed us to quantify the degree of distortion of the coordination sphere (an *S* value equal to 0 corresponds to the perfect polyhedron, while a larger value indicates a greater deviation from the ideal geometry). The relatively large *S* values (Table S1, ESI†) indicate that the coordination environment of Dy(III) centres were in a low geometrical symmetry.

Complex **2** also crystallizes in the triclinic space group $P\bar{1}$. The crystal structure and the local coordination geometry around Dy(III) ions were nearly identical to that of complex **1**, except for the presence of two $CH_2ClCH_2Cl$ instead of four $CHCl_3$ molecules as the lattice solvent. Accordingly, the bond lengths of Dy–O and Dy–Dy in complex **2** were nearly the same as those in complex **1** (Table S2, ESI†). The intramolecular Dy1–Dy1′ distance and the average Dy–O distance were 3.8347(5) Å and 2.385(3) Å in **1**, 3.8452(3) Å and 2.377(2) Å in **2**, respectively. The atoms Dy1, Dy1′, O1 and O1′ were on a horizontal plane in both complexes **1** and **2**, with only a slight difference in the angles (Table S2, ESI†) and the degree of distortion of the quadrilateral formed by two Dy and two phenoxy O atoms (Tables S2 and S3, ESI†). In complex **1**, the O1–Dy1–O1′ angle was 67.34(12)° and the Dy1–O1–Dy1′ angle was 112.66(12)°, while the O1–Dy1–O1′ angle and Dy1–O1–Dy1′ angle were 66.68(7)° and 113.32(7)° respectively in **2**. This means that complex **2** has a more inclined quadrilateral formed by Dy1, Dy1′, O1 and O1′ atoms. In addition, the *S* parameters of Dy(III) centres in **2** also displayed relatively large values (Table S1, ESI†) according to the ideal biaugmented tri-

 

gonal prism. These values were nearly the same as those of **1** and also indicative of a low geometrical symmetry and obvious deviation from the ideal $C_{2v}$ symmetry.

The Dy-DMOP units of complexes **1** and **2** were "stacked" along the crystallographic *a*-axis in a way depicted in Fig. 2 and Fig. S1 (ESI†), respectively. Hydrogen-bond interactions and π-bond interactions were found in both complexes and are marked in detail in Fig. 2, Fig. S2 and Table S4 (ESI†). The hydrogen bonds were mainly composed of a chlorine atom of $CHCl_3$/$CH_2ClCH_2Cl$ and a carbon atom of DBM and DMOP. The shortest intermolecular Dy···Dy distances between the neighbouring [DyDy] units for **1** and **2** were 10.6974(8) Å and 10.4264(4) Å, respectively, suggesting that the intermolecular dipole–dipole interaction could be negligible compared to the intramolecular interaction.

Despite complexes **1** and **2** possessing nearly the same core structures, a further close inspection of them showed their slightly different bond lengths and angles. These discrepancies were most likely due to the different lattice solvents, which influence the intermolecular stacking and consequently perturb the first coordination sphere, albeit they are remote from the spin centres.

In order to prepare the desolvated sample, complex **1** was placed in a vacuum oven maintained at 80 °C for drying for 24 h, with the corresponding TG analysis (Fig. S3 and S4, ESI†) confirming that the lattice solvent molecules had been completely removed, leading to $[Dy_2(DMOP)_2(DBM)_4]$ (**de1**). Unfortunately, the single-crystal X-ray diffraction data of **de1** were not obtained for the crystal cracking upon drying. Alternatively, powder X-ray diffraction measurement was then performed on **de1** and confirmed that the frame structure was maintained, albeit with the existence of a slightly different pattern compared with complex **1** (Fig. S5, ESI†), which was also found in other research studies and was mostly attributed to the release of the lattice solvents.[19] Interestingly, the recrystallizing of complex **de1** in $CHCl_3$ solvent at room temperature could recover complex **1**, as confirmed by X-ray diffraction measurements and TG analysis (Fig. S5 and S6, ESI†). These results show that the desolvation–resolvation process between **1** and **de1** is reversible.

### Magnetic behaviour and theoretical calculations

The thermal ($T$) dependence of the molar magnetic susceptibilities ($\chi_M$) of all three samples were measured in an applied direct current (dc) field of $H$ = 1000 Oe in the temperature range of 2–300 K. Fig. 3 shows the plots of $\chi_M T$ *versus* $T$ for **1**, **2** and **de1**. At room temperature, the $\chi_M T$ values were 28.24 (**1**), 28.38 (**2**) and 28.53 (**de1**) cm$^3$ K mol$^{-1}$, which were in good agreement with the theoretical value of 28.34 cm$^3$ K mol$^{-1}$ for two free Dy(III) ions ($^6H_{15/2}$, $S$ = 5/2, $L$ = 5, $g$ = 4/3). Upon cooling, the $\chi_M T$ product decreased gradually, which was likely due to the thermal depopulation of the Dy(III) Stark sublevels and/or intermolecular antiferromagnetic behaviour. Below 30 K, the $\chi_M T$ product decreased significantly until 2 K, indicating a significant magnetic anisotropy of Dy(III)[1c] and/or weak intramolecular antiferromagnetic interactions through the phenoxy bridge. Plots of $M$ *versus* $H/T$ below 8 K for complex **1** (Fig. 3, inset) show a rapid increase in the magnetization at low fields. The magnetization reached a value of 11.6$N\beta$ at 7 T at 2 K, which was much lower than the theoretical saturation value of 20$N\beta$ for the $Dy_2$ dimer. The field dependence of the magnetization for complexes **2** and **de1** between 2 and 8 K are shown in Fig. S7–S9 (ESI†). The unsaturated magnetization together with the non-superposition of the $M$ *versus* $H/T$ curves suggest a large magnetic anisotropy and the presence of low lying excited states in this system.

To explore the intramolecular magnetic interactions of these dinuclear complexes, magnetic measurements for the Gd(III) analogue (complex **4**) were carried out. The magnetic

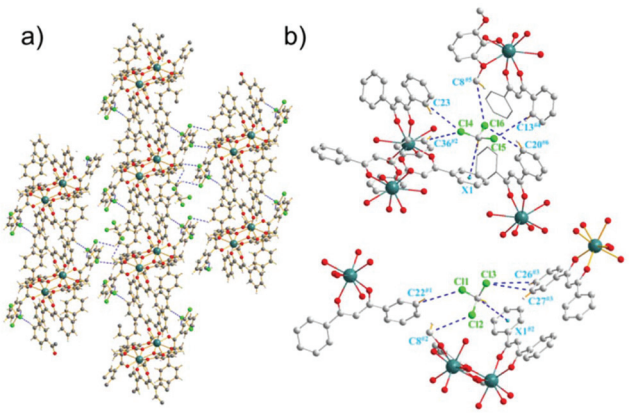


**Fig. 2** (a) Crystal packing of **1** along the *a*-axis. Dy, dark blue; O, red; C, grey; H, white; Cl, green. (b) Views showing the C–H···π interactions and intermolecular H–C···Cl interactions among the crystallographically equivalent Dy–DMOP units of **1** (hydrogen atoms have been omitted for clarity; symmetry codes: #1: 1 – $x$, 1 – $y$, $z$; #2: 1 – $x$, 1 – $y$, 1 – $z$; #3: $x$ – 1, $y$, $z$; #4: 1 – $x$, –$y$, –$z$; #5: $x$, $y$, $z$ – 1; #6: 1 + $x$, $y$, $z$).

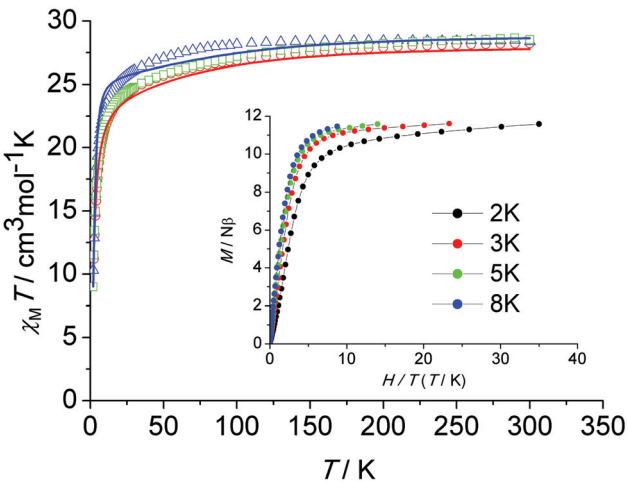


**Fig. 3** The $\chi_M T$ data measured on powdered samples under a magnetic field $H$ = 1000 Oe for **1** (red circles; red line, best fit), **2** (blue triangles; blue line, best fit) and **de1** (green diamonds). Inset: $M$ *versus* $H/T$ plot for **1** at indicated temperatures.

properties were analyzed by spin Hamiltonian $H = -JS_{Gd1}\cdot S_{Gd2}$, where $J$ is the exchange coupling constant and $S_{Gd1}$ and $S_{Gd2}$ are the spin operators. The temperature dependence of the $\chi_M T$ product for complex **4** combined with a plot of $\chi_M^{-1}$ *vs.* $T$ is shown in Fig. S10 (ESI†). Least-squares fitting of the experimental data with eqn (S1)† leads to $J = -0.035$ cm$^{-1}$ and $g = 2.0$ ($R = 1.7 \times 10^{-3}$, defined as $\sum[(\chi_M T)_{calc} - (\chi_M T)_{obs}]^2/\sum[(\chi_M T)_{obs}]^2$). The temperature dependence of $\chi_M^{-1}$ obeys the Curie–Weiss law in the 50–300 K range (Fig. S11, ESI†) with the Curie constant $C$ of 16.50 cm$^3$ K mol$^{-1}$ and Weiss constant $\theta$ of −2.2 K, indicating a weak antiferromagnetic interaction between the Gd(III) centres. This may be similar in Dy(III) complexes.

To gain further insights into the magnetic properties of our complexes, complete-active-space self-consistent field (CASSCF) based *ab initio* calculations were performed using *MOLCAS 7.8*.[20] The total exchange coupling constants $J$ (including dipolar $J_{dip}$ and exchange $J_{ex}$) and the pseudospin $\hat{S} = 1/2$ of the Dy(III) ions were used in the calculations. The calculated and experimental magnetic susceptibilities of complexes **1** and **2** are shown in Fig. 3, where the fits are all close to the experimental data in the whole temperature range. The Dy(III)–Dy(III) interactions in the two complexes within Lines' model[21] were both antiferromagnetic. The best fit results gave $J_{ex1} = -1.25$ cm$^{-1}$, $J_{dip1} = -2.77$ cm$^{-1}$ for complex **1** and $J_{ex2} = -3.00$ cm$^{-1}$, $J_{dip2} = -2.51$ cm$^{-1}$ for complex **2**. Accordingly, the overall antiferromagnetic exchange coupling $J_1$ of −4.02 cm$^{-1}$ for complex **1** was weaker than the $J_2$ of −5.51 cm$^{-1}$ for complex **2** (Table S5, ESI†).

To investigate the magnetization dynamics of the present systems, alternating current (ac) magnetic susceptibility measurements were performed on complex **1** in the temperature range 2–16 K under a zero dc field at frequencies between 1 and 1000 Hz (Fig. 4, upper figure and Fig. S1, ESI†). The out-of-phase ($\chi''$) component of the ac susceptibility (Fig. 4, upper figure) clearly exhibits temperature-dependent peaks with one maximum. Additionally, the frequency dependence of the maximum in association with a single relaxation process appears clearly on the plot of the $\chi''$ *versus* the frequency between 1 and 1000 Hz (Fig. 4, lower figure and Fig. S12, ESI†). The single relaxation mode in the frequency-dependent ac susceptibility is ascribed to there being only one crystallographically independent Dy(III) ion in the centrosymmetric complex.

The graphical representation of $\chi''$ *vs.* $\chi'$ (Cole–Cole plot)[22] in the temperature range 2–12 K further confirmed the single thermally-activated relaxation process (Fig. 5, Table S6, ESI†). The data could be fitted using a generalized Debye model.[23] For temperatures higher than 4 K, symmetric semicircles were obtained. The parameter $\alpha$, indicating deviation from the pure Debye model, was lower than 0.2, which confirmed that the magnetization relaxed with a unique single characteristic time. In addition, as observed for the frequency-dependent ac susceptibility below 4 K, the antiferromagnetic interaction between the two Dy(III) ions resulted in a drop of the out-of-phase susceptibility,[24,25] $\chi''$, and a slight asymmetry in the Cole–Cole plot appears as well as an increased $\alpha$ value.

The relaxation time was extracted and fitted to the Arrhenius law $\tau = \tau_0 \exp(U_{eff}/k_B T)$. The effective energy barrier ($U_{eff}$) and the pre-exponential factor ($\tau_0$) were obtained with $U_{eff}/k_B = 97.8$ K ($\tau_0 = 3.4 \times 10^{-8}$ s) from the high-temperature regime (10–11 K) of the relaxation where it was thermally induced (Table 1 and Fig. 6).

In order to probe the impact of intramolecular interactions on the slow relaxation of the magnetization and the possible quantum tunnelling effects occurring in these SMMs, diluted samples of **1** were prepared in $DyCl_3\cdot 6H_2O/YCl_3\cdot 6H_2O$ molar ratios of 1 : 4, 1 : 9 and 1 : 19 (1.0 mmol in total, instead of 1.0 mmol of $DyCl_3\cdot 6H_2O$) and labelled as **1a**, **1b** and **1c**, respectively. The corresponding $Y_2$ congener (complex **3**) was

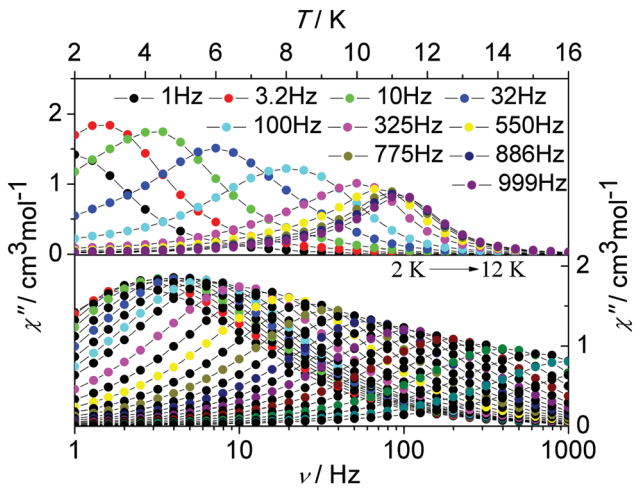


Fig. 4 Temperature (up) and frequency $\nu$ (down, logarithmic scale) dependence of out-of-phase ($\chi''$) ac susceptibility in the temperature range 2–16 K for **1** under a zero dc field.

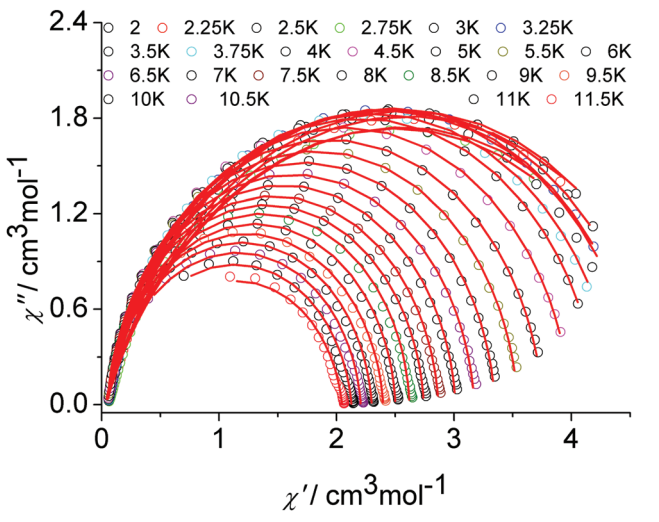


Fig. 5 Cole–Cole (Argand) plot for **1** obtained using the ac susceptibility data. The solid lines correspond to the best fit obtained with a generalized Debye model under a zero dc field.

Table 1 Energy barriers obtained from the Arrhenius law fitting of the frequency-dependent ac susceptibility data in a zero dc field

| Complex | $U_{eff}/k_B$ [K] | $\tau_0$ [s] |
|---|---|---|
| **1** | 97.8 | $3.4 \times 10^{-8}$ |
| **2** | 147.2 | $2.3 \times 10^{-8}$ |
| **de1** | 194.0 | $6.0 \times 10^{-9}$ |

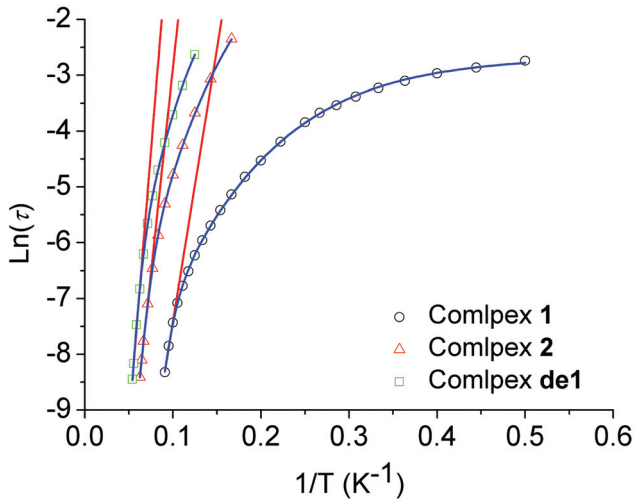


Fig. 6 Plot of ln($\tau$) *versus* 1/$T$ at a zero dc field for **1**, **2** and **de1**. The red lines represent a pure Arrhenius fitting at the high-temperature linear region for **1**, **2** and **de1** at a zero dc field. The blue lines represent the fitting of the frequency-dependent data by eqn (1) for **1**, **2** and **de1** at a zero dc field.

isostructural with **1**. As confirmed by single-crystal X-ray diffraction. Alternating current (ac) susceptibility measurements were performed on polycrystalline samples in the SQUID magnetometer. The temperature dependence of the ac susceptibility in the 2–16 K range was measured for all of the diluted samples at various frequencies and dc fields (Fig. 7, Fig. S13–S16, ESI†). The measurements on diluted Dy2 samples under a zero applied dc field exhibited clear temperature-dependent peaks below 16 K, indicating SMM behaviour. It is very interesting that they displayed different behaviours below 5 K; as can be seen in the data of the different diluted concentration sample under 100 Hz in Fig. 7 for comparison. A single

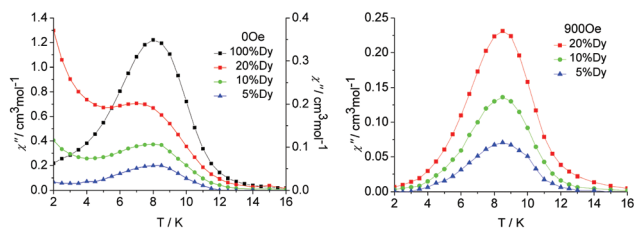


Fig. 7 Temperature dependence of the out-of-phase susceptibility ($\chi''$) at 100 Hz and applied fields of (left) 0, and (right) the optimum field 900 Oe for the diluted samples **1a**, **1b** and **1c**.

maximum of peak was observed at ~8 K for all samples, which was indicative of their same origin of slow magnetic relaxation; however, a tail of the temperature-dependent peak was observed for diluted samples below 5 K (Fig. 7, left). Such a tail of $\chi''$ is usually indicative of QTM *via* degenerate $\pm M_J$ energy levels.[26–28] However, for most SMMs, the efficient suppression of QTM with the decreased $\chi''$ will be seen in the magnetic measurements of diluted samples, because the increased intermolecular distance leads to reduced magnetic dipole–dipole interactions that usually induce QTM.[29] Whereas in this case, we observed the increase of $\chi''$ in diluted samples (Fig. S15, ESI†) and the intensity of the tail increased with the increasing percentage of Dy dilution in **1a**, **1b** and **1c**, which is consistent with the increase in the major species YDy. This clearly demonstrates that the increasing tails of $\chi''$ seen in our system were related to the QTM process accompanying the single-ion relaxation behaviour of the [Dy–Y] component after decoupling the Dy–Dy interaction in diluted samples.[27] Conversely, the QTM was negligible in the original undiluted sample with the intramolecular interaction, which revealed an effective suppression of the QTM of the intramolecular Dy–Dy coupling. A similar phenomenon has been observed in a few decoupling Dy2 SMM systems.[9]

In order to reduce the QTM usually found in mononuclear lanthanide SMMs, one efficient way is by applying a static dc field to remove the degeneracy of the $\pm M_J$ energy levels, consequently preventing the tunnelling of electrons from the $+M_J$ state to the $-M_J$ state. To fully suppress the tunnelling effects, optimum dc field measurements were carried out at 2 K and optimum fields of 900 Oe were found for 5%, 10% and 20% Dy(III) dilution (Fig. S16 and S17, ESI†). Subsequent ac measurements were carried out under the optimum field 900 Oe (Fig. 7, right). A clear single relaxation peak without the presence of a tail was observed in the out-of-phase susceptibility plots, which confirmed the effective suppression of QTM. The intensities of the peaks gave an indication that the major species present in the diluted samples was the YDy complex.

In order to probe the impact of the lattice solvents on their dynamic magnetic relaxations, we carried out magnetic measurements on the desolvated sample **de1** (Fig. 8, Fig. S18, ESI†). It was interesting to find that they displayed significantly different magnetic relaxation behaviours. For **de1**, the ac magnetic susceptibility data collected under a zero applied dc field showed that the temperature-dependent $\chi''$ peaks appear at a higher temperature of 19 K (Fig. 8). The effective energy barrier was nearly doubly improved to $U_{eff}/k_B$ = 194.0 K compared to 97.8 K for **1**. To understand this result, ac magnetic measurements were carried out under a zero applied dc field on the diluted **de1** similar with **1**, denoted as **de1b** (Fig. S19 and S20, ESI†). Indeed, a similar SMM behaviour was observed for **de1b**, which indicated their same origins of slow magnetic relaxation (Fig. 10). In other words, for both diluted and undiluted samples, the effective energy barrier could be enhanced by a factor of about two after desolvation. In addition, compared to **de1**, a pronounced QTM at low temp-

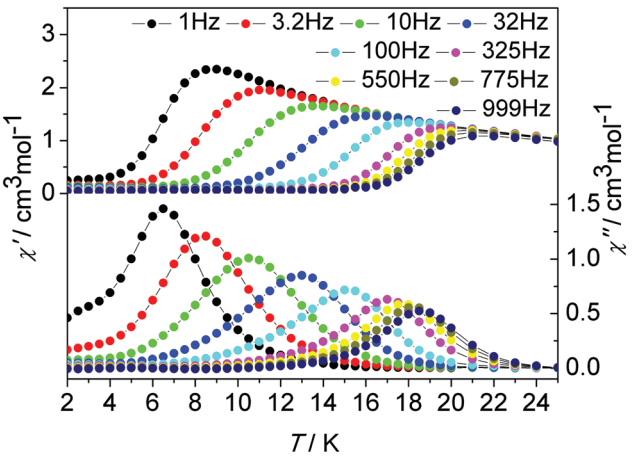


Fig. 8 Temperature dependence of the in-phase $\chi'$ and out-of-phase $\chi''$ ac susceptibility signals under a zero dc field for **de1**.

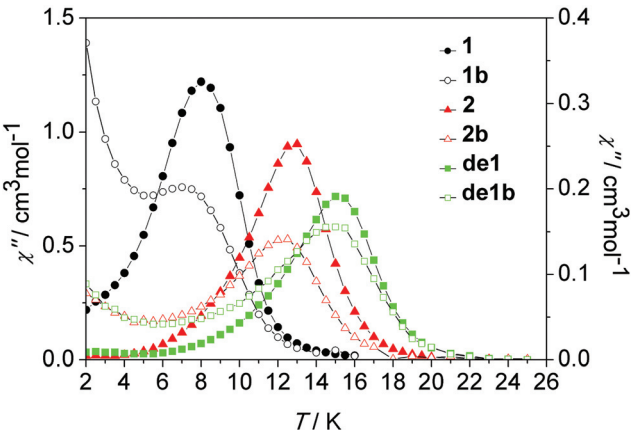


Fig. 10 Temperature dependence of the out-of-phase susceptibility ($\chi''$) at 100 Hz under a zero dc field for **1**, **1b**, **2**, **2b**, **de1** and **de1b**.

erature was observed in the diluted samples, like aforementioned found in **1** and **1b**. The different magnetization relaxation behaviours of **1** and **de1** could most likely be attributed to the loss/gain of the crystallization solvent, which probably induces a subtle structural rearrangement around Dy(III) ions,[30] albeit the lattice solvent did not link to the Dy(III) centres directly.

Although our attempt to obtain the crystal structure of **de1** ultimately failed, complex **2** with a replaced solvent $CH_2ClCH_2Cl$ was prepared successfully. Its geometrical structures and magnetic properties were characterized and comparably studied. Complexes **1** and **2** are isostructural with very similar core structures of the dinuclear Dy2 moiety; however, the lattice solvents induce slightly structural differences, and indeed lead to a dramatically distinct dynamic magnetic relaxation. The ac magnetic susceptibilities of complex **2** were measured in the temperature range 2–23 K under a zero dc field at frequencies between 1 and 1000 Hz (Fig. 9 and

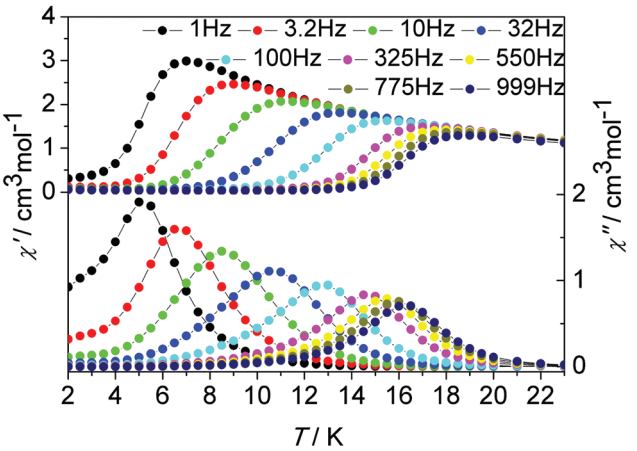


Fig. 9 Temperature dependence of the in-phase ($\chi'$) and out-of-phase ($\chi''$) ac susceptibility signals under zero dc field for **2**.

Fig. S21, ESI†). The $\chi''$ peaks could be observed at a higher temperature of near 17 K, compared to 11 K for complex **1**, and close to that found in complex **de1** (Fig. 9, 10 and Fig. S21–S23, ESI†). The effective energy barrier of complex **2** extracted from Arrhenius law was $U_{eff}/k_B$ = 147.2 K (14–16 K, $\tau_0 = 2.3 \times 10^{-8}$ s; Table 1, Fig. 5 and Fig. S21, ESI†).

As shown in Fig. 10, nearly identical $\chi''$ peaks under the same frequency between the diluted and undiluted samples of **1** and **2** series were observed, respectively, which was indicative of their pure and same molecular origin of magnetic relaxations. The increasing tails at a low temperature regime for the diluted systems of **1** and **2** reveal a pronounced QTM occurring after intramolecular decoupling of the exchange interaction. The Dy–Dy coupling plays a critical role in suppressing QTM. The impact of lattice solvents on their dynamic magnetic relaxations was also very apparent. Under the same 100 Hz, the observed $\chi''$ peak at 8 K of **1** increased to 15 K for **de1** and 13 K for **2**, accompanying the increasing energy barriers (Table 1).

In addition, the plots of $\ln(\tau)$ *versus* $1/T$ under a zero dc field exhibited an obvious curvature, which has been observed in few SIMs[31] and indicates that perhaps other relaxation pathways are also operative, so the $U_{eff}$ values of these samples **1**, **2** and **de1** were obtained by fitting the magnetic data with eqn (1). The fits with eqn (1) were in good agreement with the data over the whole temperature regime with $U_{eff}/k_B$ = 157.2 K, $\tau_0 = 2.5 \times 10^{-6}$ s for **1**; $U_{eff}/k_B$ = 190.8 K, $\tau_0 = 2.0 \times 10^{-9}$ s for **2** and $U_{eff}/k_B$ = 258.4 K, $\tau_0 = 2.4 \times 10^{-10}$ s for **de1** (Fig. 5 and Table S7, ESI†). These results once again prove that the $U_{eff}$ of **de1** is nearly twice as large as that of **1** and the $U_{eff}$ value also increased from **1** to **2**.

$$1/\tau = 1/\tau_{QTM} + CT^n + {\tau_0}^{-1} \exp(-U_{eff}/\kappa T) \quad (1)$$

To further probe the dynamic magnetic properties, hysteresis loop measurements were carried out over the 1.8–4 K temperature range for samples **1**, **1b**, **2**, **2b**, **de1** and **de1b** (Fig. 11 and 12). Complex **1** did not show a hysteresis loop

 

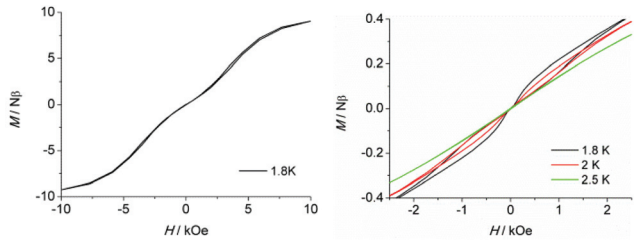


**Fig. 11** Field dependence of the normalized magnetization of samples **1** (left) and **1b** (right) between 1.8 and 2.5 K at a sweep rate of 200 Oe $s^{-1}$.

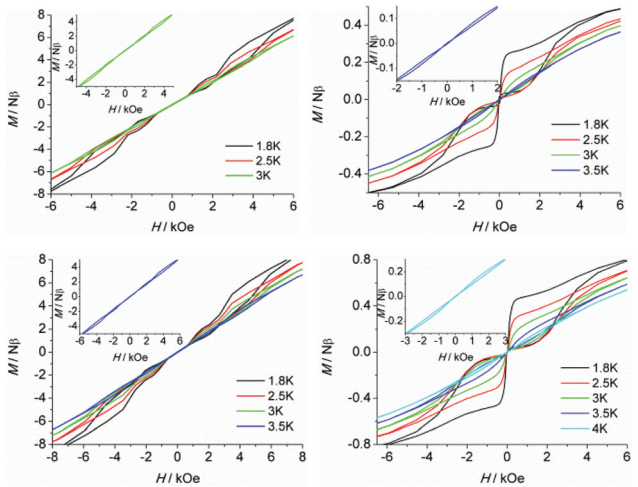


**Fig. 12** Field dependence of the normalized magnetization of samples **2** (top left), **2b** (top right), **de1** (bottom left) and **de1b** (bottom right) between 1.8 and 4 K at a sweep rate of 200 Oe $s^{-1}$. Inset: *M versus H* plots for each at the highest temperature.

(Fig. 11) at 1.8 K. However, the *M versus H* plot for the diluted sample of **1b** with the Y : Dy molar ratio of 1 : 9 displayed a butterfly-shaped hysteresis loop at 1.8 K under a sweep rate of 200 Oe $s^{-1}$ (Fig. 11, right). Upon raising the temperature, the openings in the hysteresis of complex **1b** become narrow and then nearly closed at 2.5 K. The opening of the hysteresis loop after the dilution of **1** indicated that the intermolecular magnetic dipole–dipole interactions play a significant role in the dynamic relaxation and suggests that the memory effect mainly comes from the magnetic relaxation of a single Dy(III) ion. A large thermal barrier and considerably slower tunnelling rate were observed with the **de1** sample; therefore an expected "S-shaped" hysteresis was observed with a large opening, even when the temperature reached up to 3.5 K (Fig. 12, bottom left). The tunnel resonance step at $H = \pm 0.3$ T could be clearly observed, which corresponded to an exchange-bias field associated with a spin flip of the antiferromagnetically coupled Dy(III) spins. Conversely, in the case of the **de1b** sample (Fig. 12, bottom right), only one large step under a zero field was observed, which was responsible for the zero-field tunnelling. This is consistent with the phenomenon often observed in lanthanide systems.[32] The decreased step at ~0.3 T was the result of a decoupling system associated with the presence of YDy species in diluted samples. As expected, complex **2** with a relatively higher $U_{eff}$ showed a significantly increased hysteresis temperature compared with **1**, and the opening of hysteresis for **2** was retained until the temperature of 3 K (Fig. 12, top left). Similarly, there was only one large step under a zero field in the case of the diluted **2b** sample (Fig. 12, top right), which stemmed from the decoupling system with the decreasing exchange-biased interaction. It is worth mentioning that the diluted samples of **1**, **2** and **de1** resulted in a higher (0.5 K increase) hysteresis temperature compared to the undiluted samples. This was attributed to the larger intermolecular separation in the diluted samples, which consequently reduced the dipole–dipole interactions usually favouring QTM.

The magnetic coupling interaction constant $J$ could also be obtained by a method based on the Zeeman effect. Considering that the steps on the hysteresis curves are the consequence of a level-crossing between the ground state and the first excited state of the dimer, eqn (2) could be applied to calculate the $J$ values.[33]

$$H_{cross} = -J/2g\beta \quad (2)$$

The first derivative of magnetization revealed that the crossing field of **2** was 2.9 kOe (Fig. S24 and 25, ESI†). Thus, $J_2$ was obtained as −5.3 $cm^{-1}$ when $g = g_z = 19.778$, which is well consistent with the above-mentioned results obtained *via ab initio* calculations (Table S8, ESI†).

The loss/gain and replacement of the crystallization solvents in samples **1**, **de1** and **2** could lead to significant different magnetic properties, albeit they did not ligate to Dy(III) directly. This was most likely due to the subtle structural changes induced by the different packing structures through hydrogen bonds or π–π interactions.[34,35] The main difference between the crystal structures of **1** and **2** arises from the unbonded solvent molecules within the lattice. Recent studies have indicated that non-bonded co-crystallized solvent molecules could influence directly the structural environment of the spin centre, which may have a dramatic impact on the dynamic magnetic relaxations in a few transition metal- or lanthanide-based SMMs or MOF-type SMMs.[15,36] For lanthanide-based SMMs, an extreme sensitivity of the dynamic relaxation to the coordination environmental, even remote from the first coordination sphere, was indeed observed.[37,38]

Although the lattice solvent did not coordinate to the Dy(III) centre directly, a slight difference in coordination surrounding the Dy(III) ions could be observed, as aforementioned in the structural analysis. As shown in Fig. S26 (ESI†), the first coordination spheres of **1** and **2** overlap well, but some peripheral fragments beyond the first coordination sphere indeed show a non-negligible difference, such as the methyl of the methoxyl on DMOP and the benzene rings of the peripheral β-diketonate ligands, which leads to different O–Dy–O angles

with a range of 0.01°–3.38° in the first coordination sphere (Table S2, ESI†). These differences were most likely due to the different intermolecular stacking caused by the different lattice solvents with hydrogen bonds and might be responsible for their different magnetic relaxations.[30]

Further insights into the electronic structure and magnetic blocking in the present dysprosium complexes were obtained *via ab initio* calculations. Generally, the effective relaxation barrier of an Orbach process is comparable with the energy difference of the ground and first excited states. CASSCF calculations on two types of individual Dy(III) fragments for each of complexes **1** and **2** on the basis of X-ray determined geometries were carried out with *MOLCAS 7.8*[20] and *SINGLE_ANISO*[39] programs (Fig. S28 and see computation details in the ESI†). The lowest spin–orbit energies and the effective *g* tensors of the ground Kramer's doublets on the dysprosium sites as strongly axial for complexes **1** and **2** are shown in Table S9 (ESI†). The calculated $g_z$ values of the Dy(III) fragments of **1** and **2** were close to 20 ($g_z$ = 19.769 for **1** and $g_z$ = 19.778 for **2**), which show that the Dy(III)–Dy(III) exchange interactions for each of them can be approximately regarded as an Ising type. However, complex **1** has a larger transverse anisotropy component than **2** as indicated by the calculated $g_x$, $g_y$ values of 0.008, 0.028 for **1** and 0.004, 0.016 for **2**, respectively. In particular, the magnetic axiality ($g_Z/g_{X,Y}$) of the ground state for **2** is almost one order larger than that for **1**, which might be the source of their different magnetic relaxation behaviours.[13c] In addition, the obtained energy gaps at 153.6 K (106.7 $cm^{-1}$) and 193.4 K (134.3 $cm^{-1}$) between the ground and the first excited states in **1** and **2** were close to the values fitted with eqn (1) over the whole temperature regime. The main magnetic axes on two Dy(III) of each complex are parallel and opposite, as indicated in Fig. S28 (ESI†), where the magnetic axes on Dy(III) for the two complexes had similar directions. We also give the exchange energies and the main values of $g_z$ for the lowest two exchange doublets of two complexes in Table S10 (ESI†). The $g_z$ values of the ground exchange states for all the complexes were equal to 0, which confirmed that the Dy(III)–Dy(III) couplings were antiferromagnetic. The simulated main magnetic axes of Dy ions in each complex are depicted in Fig. S29 (ESI†). The Dy–Dy magnetization axis formed an angle of 79.4° with the line of Dy–Dy direction for complex **1**, which was larger than the angle of 76.8° for complex **2**. Moreover, in complex **1**, the magnetization axis formed an angle of 4.2° with the plane (O1–Dy1–O1′) and an angle of 16.7° with the equatorial plane (O1–O1′–O2′–O3–O5), which, respectively, were 3.6° and 14.3° in complex **2**. The angles between the equatorial plane (O1–O1′–O2′–O3–O5) and the vertical plane (O4–O6–O7) were 84.4° and 87.0° for **1** and **2**, respectively (Fig. S29, ESI†). These results indicate that the orientation of the magnetization axis is closer to the orientation of Dy–Dy in complex **2** than that in complex **1**. Consequently, complex **2** has a stronger intramolecular antiferromagnetic interaction as aforementioned and displays a more remarkable SMM behaviour.

# Conclusions

We have shown that the magnetic anisotropy of a dinuclear dysprosium complex $[Dy_2(DMOP)_2(DBM)_4(CHCl_3)_4]$ (**1**) can be significantly improved by removing the lattice $CHCl_3$ molecule or by replacing it with $CH_2ClCH_2Cl$ providing $[Dy_2(DMOP)_2(DBM)_4(C_2H_4Cl_2)_2]$ (**2**). Further studies on the dynamic magnetic relaxation processes of these complexes and their diluted samples indicated that the slow magnetic relaxations were mostly derived from the single-ion anisotropy. Interestingly, a dramatic increase in $U_{eff}$ and the hysteresis temperature could be realized by only releasing or replacing the unbonded solvent molecules. This experimental observation provides new insight for designing lanthanide-based SMMs, which could be obtained by manipulating the guest molecules either in low dimensional systems or MOF materials. Meanwhile, it should be noted that the SMMs with solvent molecules should be treated with caution in magnetic measurements owing to the possible influence on their dynamic relaxation.

# Experimental section

### General information

All the solvents were used as received without further purification. Other chemicals were commercially available and generally used as supplied. Elemental (C and H) analyses were performed with a PerkinElmer 2400 analyzer.

### Single-crystal X-ray diffraction

Crystal data for complexes **1–4** were collected on a Xcalibur, Eos, Gemini diffractometer with Mo Kα radiation ($\lambda$ = 0.71073 Å). Complexes **1**, **3** and **4** were collected at 293(2) K, while **2** was collected at 180(2) K. The structures of complexes **1–4** were solved by direct methods and refined on $F^2$ by full-matrix least-squares using the *SHELXTL-2014* program and Olex2.[40] All non-hydrogen atoms were refined with isomorphous displacement parameters. All crystallographic data for complexes **1–4** are summarized in Table 2, and selected bond lengths and angles for complexes **1** and **2** are tabulated in Table S2 (ESI†).

### Powder X-ray crystallography

Powder X-ray data were recorded at room temperature on a Bruker D8 diffractometer using Cu Kα ($\lambda$ = 1.5406 Å) radiation. The accelerating voltage and the applied current were 40 kV and 20 mA, respectively.

### Magnetic measurements

The magnetic susceptibilities of the complexes were measured using a Quantum Design VSM superconducting quantum interference device (SQUID) magnetometer. Data were corrected for the diamagnetism of the samples using Pascal constants and the sample holder by measurement.

 

Table 2 Crystallographic details for complexes **1–4**

| Complex | **1** | **2** | **3** | **4** |
|---|---|---|---|---|
| Empirical formula | $C_{80}H_{66}Cl_{12}Dy_2O_{14}$ | $C_{80}H_{70}Cl_4Dy_2O_{14}$ | $C_{80}H_{66}Cl_{12}Y_2O_{14}$ | $C_{80}H_{66}Cl_{12}Gd_2O_{14}$ |
| FW (g mol$^{-1}$) | 2001.73 | 1722.16 | 1854.55 | 1991.23 |
| Crystal system | Triclinic | Triclinic | Triclinic | Triclinic |
| Space group | $P\bar{1}$ | $P\bar{1}$ | $P\bar{1}$ | $P\bar{1}$ |
| Temperature (K) | 293(2) | 180(2) | 293(2) | 293 |
| $a$ (Å) | 11.7531(9) | 11.4039(3) | 11.7403(7) | 11.765 |
| $b$ (Å) | 13.8438(10) | 13.0199(5) | 13.8267(8) | 13.856 |
| $c$ (Å) | 13.9872(7) | 13.9897(5) | 13.9874(9) | 14.010 |
| $\alpha$ (°) | 102.801(6) | 70.393(3) | 103.008(5) | 102.87 |
| $\beta$ (°) | 91.679(5) | 71.631(3) | 92.037(5) | 91.29 |
| $\gamma$ (°) | 108.946(7) | 75.913(3) | 108.773(5) | 108.64 |
| $V$ (Å$^3$) | 2086.3(2) | 1834.87(12) | 2080.2(2) | 2098.7 |
| $\rho_{cacd}$ (Mg m$^{-3}$) | 1.593 | 1.559 | 1.480 | 1.575 |
| $\mu$ (mm$^{-1}$) | 2.222 | 2.231 | 1.834 | 2.008 |
| $F$(000) | 994 | 862 | 940 | 990.0 |
| Independent relections | 10 517 | 9451 | 9412 | 9287 |
| $R_{int}$ | 0.0384 | 0.0350 | 0.0330 | 0.0328 |
| $R_1{}^a$ [$I > 2\sigma(I)$] | 0.0498 | 0.0348 | 0.0630 | 0.0431 |
| w$R_2{}^b$ (all data) | 0.1236 | 0.0694 | 0.1707 | 0.1166 |
| Goodness of fit on $F^2$ | 1.030 | 1.092 | 1.025 | 1.082 |
| CCDC numbers | 1411817 | 1411818 | 1413255 | 1413256 |

$^a R_1 = \sum||F_o| - |F_c||/\sum|F_o|$. $^b wR_2 = \sum[w(F_o^2 - F_c^2)^2]/\sum[w(F_o^2)^2]^{1/2}$.

### Synthesis of $[Dy_2(DMOP)_2(DBM)_4(CHCl_3)_4]$ (1) and $[Dy_2(DMOP)_2(DBM)_4(C_2H_4Cl_2)_2]$ (2)

To a stirred solution of 1,3-diphenylpropane-1,3-dione (DBM) (0.449 g, 2.0 mmol) and 2,6-dimethoxyphenol (DMOP) (0.154 g, 1.0 mmol) in 22 mL of EtOH, an alcoholic solution (10 mL) of sodium hydroxide (0.120 g, 3.0 mmol) was added dropwise, resulting in a black solution. After that an alcoholic solution (7.5 mL) of $DyCl_3{\cdot}6H_2O$ (0.377 g, 1.0 mmol) was added dropwise to the above solution, resulting in a brown precipitate. The reaction mixture was refluxed and stirred for a further period of 4 h and was then cooled and filtered. The residue obtained was washed with water and ethyl alcohol. And then, after drying at 50 °C under vacuum conditions, we obtained a grey powder. Yield: 0.568 g. The powder was dissolved in $CHCl_3$ and 1,2-dichloroethane ($C_2H_4Cl_2$), respectively, and kept for crystallization under slow evaporation conditions. After 3–4 days, pure yellowish crystals of **1** and **2** were obtained and collected. For **1**, yield: 0.382 g (51.2%). Elemental analysis (wt%) calcd for $C_{80}H_{66}Cl_{12}Dy_2O_{14}$: C 47.98, H 3.30; found: C 48.01, H 3.26. For **2**, yield: 0.297 g (46.3%). Elemental analysis (wt%) calcd for $C_{80}H_{70}Cl_4Dy_2O_{14}$: C 55.78, H 4.07; found: C 55.80, H 4.16.

### Synthesis of $[Y_2(DMOP)_2(DBM)_4(CHCl_3)_4]$ (3)

The preparation of this complex followed the same procedure as for **1** except that $YCl_3{\cdot}6H_2O$ (0.303 g, 1.0 mmol) was used as the starting material instead of $DyCl_3{\cdot}6H_2O$. We obtained a grey powder. Yield: 0.503 g. The powder was dissolved in $CHCl_3$, and kept for crystallization under slow evaporation conditions. After 3–4 days, pure yellowish crystals of **3** were obtained and collected. Yield: 0.343 g (50.6%). Elemental analysis (wt%) calcd for $C_{80}H_{66}Cl_{12}Y_2O_{14}$: C 51.78, H 3.56; found: C 51.81, H 3.65.

### Synthesis of $[Gd_2(DMOP)_2(DBM)_4(CHCl_3)_4]$ (4)

The preparation of this complex followed the same procedure as for **1** except that $GdCl_3{\cdot}6H_2O$ (0.372 g, 1.0 mmol) was used as the starting material instead of $DyCl_3{\cdot}6H_2O$. We obtained a grey powder. Yield: 0.551 g. The powder was dissolved in $CHCl_3$, and kept for crystallization under slow evaporation conditions. After 3–4 days, pure yellowish crystals of **4** were obtained and collected. Yield: 0.390 g (52.6%). Elemental analysis (wt%) calcd for $C_{80}H_{66}Cl_{12}Gd_2O_{14}$: C 48.21, H 3.31; found: C 48.18, H 3.25.

### Procedure for the synthesis of the diluted samples of complex 1, which are labelled as 1a, 1b and 1c

These diluted complexes were prepared by following the same method as that for **1** but here we used $DyCl_3{\cdot}6H_2O/YCl_3{\cdot}6H_2O$ (0.1 mmol in total, in a 1 : 4, 1 : 9, 1 : 19 moral ratio respectively) instead of 1.0 mmol of $DyCl_3{\cdot}6H_2O$. Specific details of each reaction and the characterization data of the products obtained are given below.

### Synthesis of $[Y_{1.6}Dy_{0.4}(DMOP)_2(DBM)_4(CHCl_3)_4]$ (1a)

Quantities: DBM (0.449 g, 2.0 mmol), DMOP (0.154 g, 1.0 mmol), NaOH (0.120 g, 3.0 mmol) $DyCl_3{\cdot}6H_2O$ (0.075 g, 0.2 mmol) and $YCl_3{\cdot}6H_2O$ (0.243 g, 0.8 mmol). The grey powder yield: 0.508 g and yellowish crystals yield 0.344 g (50.5%). Elemental analysis (wt%) calcd for $C_{80}H_{66}Cl_{12}Y_{1.6}Dy_{0.4}O_{14}$: C 50.98, H 3.50; found: C 51.21, H 3.45.

### Synthesis of $[Y_{1.8}Dy_{0.2}(DMOP)_2(DBM)_4(CHCl_3)_4]$ (1b)

Quantities: DBM (0.449 g, 2.0 mmol), DMOP (0.154 g, 1.0 mmol), NaOH (0.120 g, 3.0 mmol) $DyCl_3{\cdot}6H_2O$ (0.038 g, 0.1 mmol) and $YCl_3{\cdot}6H_2O$ (0.273 g, 0.9 mmol). The grey

powder yield: 0.500 g and yellowish crystals yield 0.337 g (50.2%). Elemental analysis (wt%) calcd for $C_{80}H_{66}Cl_{12}Y_{1.8}Dy_{0.2}O_{14}$: C 51.38, H 3.53; found: C 51.61, H 3.37.

#### Synthesis of $[Y_{1.9}Dy_{0.1}(DMOP)_2(DBM)_4(CHCl_3)_4]$ (1c)

Quantities: DBM (0.449 g, 2.0 mmol), DMOP (0.154 g, 1.0 mmol), NaOH (0.120 g, 3.0 mmol) $DyCl_3{\cdot}6H_2O$ (0.019 g, 0.05 mmol) and $YCl_3{\cdot}6H_2O$ (0.289 g, 0.95 mmol). The grey powder yield: 0.498 g and yellowish crystals yield 0.332 g (49.5%). Elemental analysis (wt%) calcd for $C_{80}H_{66}Cl_{12}Y_{1.9}Dy_{0.1}O_{14}$: C 51.58, H 3.55; found: C 51.11, H 3.49.

#### Synthesis of the diluted sample $[Y_{1.8}Dy_{0.2}(DMOP)_2(DBM)_4(C_2H_4Cl_2)_2]$ of complex 2, which is labelled as 2b

This diluted complex was prepared by following the same method as that for **2** but here we used $DyCl_3{\cdot}6H_2O$ (0.038 g, 0.1 mmol)/$YCl_3{\cdot}6H_2O$ (0.273 g, 0.9 mmol) (1.0 mmol in total, in a 1 : 9 moral ratio) instead of 1.0 mmol of $DyCl_3{\cdot}6H_2O$. We obtained a grey powder. Yield: 0.500 g. The powder was dissolved in 1,2-dichloroethane, and kept for crystallization under slow evaporation conditions. After 3–4 days, pure yellowish crystals of **2b** were obtained and collected. Yield: 0.283 g (49.2%). Elemental analysis (wt%) calcd for $C_{80}H_{70}Cl_4Y_{1.8}Dy_{0.2}O_{14}$: C 60.43, H 4.41; found: C 60.39, H 4.34.

#### Synthesis of solvent-free sample $[Dy_2(DMOP)_2(DBM)_4]$ of complex 1, which is labelled as de1

To maintain complex **1** at 80 °C for 24 h under vacuum conditions, the lattice solvent molecule was almost completely removed leading to complex $[Dy_2(DMOP)_2(DBM)_4]$ (**de1**). Elemental analysis (wt%) calcd for $C_{76}H_{62}Dy_2O_{14}$: C 59.88, H 4.07; found: C 59.91, H 4.15.

#### Synthesis of the diluted and solvent-free sample $[Y_{1.8}Dy_{0.2}(DMOP)_2(DBM)_4]$ of complex de1, which is labelled as de1b

To maintain complex **1b** at 80 °C for 24 h under vacuum conditions, the lattice solvent molecule was almost completely removed leading to complex $[Y_{1.8}Dy_{0.2}(DMOP)_2(DBM)_4]$ (**de1b**). Elemental analysis (wt%) calcd for $C_{76}H_{62}Y_{1.8}Dy_{0.2}O_{14}$: C 65.59, H 4.46; found: C 65.60, H 4.52.

## Conflicts of interest

There are no conflicts to declare.

## Acknowledgements

This work was supported by the NSFC (21621061, 21290171, 21571008 and 21572048), BJSFC (2122023) and National Key R&D Program of China (2017YFA0206301, 2017YFA0204903), the BNLMS (20140108), and the Heilongjiang Province (1254G045, 12541639), Heilongjiang University (JCL201605, 2017230101001473) and Natural Science Foundation of Jiangsu Province of China (BK20151542).

## Notes and references

1 (*a*) N. Ishikawa, M. Sugita, T. Ishikawa, S. Koshihara and Y. Kaizu, *J. Am. Chem. Soc.*, 2003, **125**, 8694; (*b*) S. Takamatsu, T. Ishikawa, S. Koshihara and N. Ishikawa, *Inorg. Chem.*, 2007, **46**, 7250; (*c*) J. Long, F. Habib, P. H. Lin, I. Korobkov, G. Entight, L. Ungur, W. Wernsdorfer, L. F. Chibotaru and M. Murugesu, *J. Am. Chem. Soc.*, 2011, **133**, 5319; (*d*) J.-L. Liu, Y.-C. Chen, Y.-Z. Zheng, W.-Q. Lin, L. Ungur, W. Wernsdorfer, L. F. Chibotaru and M.-L. Tong, *Chem. Sci.*, 2013, **4**, 3310; (*e*) P. Zhang, L. Zhang, C. Wang, S. Xue, S.-Y. Lin and J. Tang, *J. Am. Chem. Soc.*, 2014, **136**, 4484; (*f*) D.-D. Yin, Q. Chen, Y.-S. Meng, H.-L. Sun, Y.-Q. Zhang and S. Gao, *Chem. Sci.*, 2015, **6**, 3095; (*g*) W.-B. Sun, P.-F. Yan, S.-D. Jiang, B.-W. Wang, Y.-Q. Zhang, H.-F. Li, P. Chen, Z.-M. Wang and S. Gao, *Chem. Sci.*, 2016, **7**, 684; (*h*) S. G. McAdams, A.-M. Ariciu, A. K. Kostopoulos, J. P. S. Walsh and F. Tuna, *Coord. Chem. Rev.*, 2017, **346**, 216; (*i*) J. F. Soria, J. Vallejo, M. Castellano, J. M. Lillo, E. Pardo, J. Cano, I. Castro, F. Lloret, R. R. García and M. Julve, *Coord. Chem. Rev.*, 2017, **339**, 17; (*j*) Z. Zhu, M. Guo, X.-L. Li and J. Tang, *Coord. Chem. Rev.*, 2017, DOI: 10.1016/j.ccr.2017.10.030.

2 (*a*) R. Sessoli, D. Gatteschi, A. Caneschi and M. A. Novak, *Nature*, 1993, **365**, 141; (*b*) R. Sessoli and A. K. Powell, *Coord. Chem. Rev.*, 2009, **253**, 2328; (*c*) P. Zhang, Y.-N. Guo and J. Tang, *Coord. Chem. Rev.*, 2013, **257**, 1728; (*d*) D. N. Woodruff, R. E. P. Winpenny and R. A. Layfield, *Chem. Rev.*, 2013, **113**, 5110; (*e*) H. L. C. Feltham and S. Brooker, *Coord. Chem. Rev.*, 2014, **276**, 1; (*f*) S. Demir, I. R. Jeon, J. R. Long and T. D. Harris, *Coord. Chem. Rev.*, 2015, **289–290**, 149; (*g*) L. Ungur, S.-Y. Lin, J. Tang and L. F. Chibotaru, *Chem. Soc. Rev.*, 2014, **43**, 6894; (*h*) Y.-S. Meng, S.-D. Jiang, B.-W. Wang and S. Gao, *Acc. Chem. Res.*, 2016, **49**, 2381; (*i*) J.-H. Jia, Q.-W. Li, Y.-C. Chen, J.-L. Liu and M.-L. Tong, *Coord. Chem. Rev.*, 2017, DOI: 10.1016/j.ccr.2017.11.012; (*j*) M. Feng and M.-L. Tong, *Chem. – Eur. J.*, 2018, **24**, 1; (*k*) J.-L. Liu, Y.-C. Chen and M.-L. Tong, *Chem. Soc. Rev.*, 2018, **47**, 2431; (*l*) W.-P. Chen, P.-Q. Liao, Y. Yu, Z. Zheng, X.-M. Chen and Y.-Z. Zheng, *Angew. Chem., Int. Ed.*, 2016, **55**, 9375.

3 (*a*) J. D. Rinehart and J. R. Long, *Chem. Sci.*, 2011, **2**, 2078; (*b*) T. Pugh, V. Vieru, L. F. Chibotaru and R. A. Layfield, *Chem. Sci.*, 2016, **7**, 2128; (*c*) S. Lee and T. Ogawa, *Chem. Lett.*, 2017, **46**, 10; (*d*) M. Gysler, F. E. Hallak, L. Ungur, R. Marx, M. Hakl, P. Neugebauer, Y. Rechkemmer, Y. Lan, I. Sheikin, M. Orlita, C. E. Anson, A. K. Powell, R. Sessoli, L. F. Chibotaru and J. van Slageren, *Chem. Sci.*, 2016, **7**, 4347; (*e*) Y.-C. Chen, J.-L. Liu, W. Wernsdorfer, D. Liu,

 

L. F. Chibotaru, X.-M. Chen and M.-L. Tong, *Angew. Chem., Int. Ed.*, 2017, **56**, 4996; (*f*) L. Norel, L. E. Darago, B. Le Guennic, K. Chakarawet, M. I. Gonzalez, J. H. Olshansky, S. Rigaut and J. R. Long, *Angew. Chem.*, 2018, **130**, 1951; (*g*) Y.-S. Ding, T. Han, Y.-Q. Hu, M. Xu, S. Yang and Y.-Z. Zheng, *Inorg. Chem. Front.*, 2016, **3**, 798; (*h*) G.-J. Zhou, Y.-S. Ding and Y.-Z. Zheng, *Dalton Trans.*, 2017, **46**, 3100; (*i*) K.-X. Yu, Y.-S. Ding, T. Han, J.-D. Leng and Y.-Z. Zheng, *Inorg. Chem. Front.*, 2016, **3**, 1028; (*j*) G.-J. Zhou, T. Han, Y.-S. Ding, N. F. Chiton and Y.-Z. Zheng, *Chem. – Eur. J.*, 2017, **23**, 15617.

4 (*a*) E. Lucaccini, J. J. Baldoví, L. Chelazzi, A.-L. Barra, F. Grepioni, J.-P. Costes and L. Sorace, *Inorg. Chem.*, 2017, **56**, 4728; (*b*) G. Cucinotta, M. Perfetti, J. Luzon, M. Etienne, P.-E. Car, A. Caneschi, G. Calvez, K. Bernot and R. Sessoli, *Angew. Chem.*, 2012, **124**, 1638; (*c*) K. S. Pedersen, L. Ungur, M. Sigrist, A. Sundt, M. S. Magnussen, V. Vieru, H. Mutka, S. Rols, H. Weihe, O. Waldmann, L. F. Chibotaru, J. Bendix and J. Dreiser, *Chem. Sci.*, 2014, **5**, 1650; (*d*) T. Han, Y.-S. Ding, J.-D. Leng, Z. Zheng and Y.-Z. Zheng, *Inorg. Chem.*, 2015, **54**, 4588.

5 (*a*) C. R. Ganivet, B. Ballesteros, G. de la Rorre, J. M. Clemente-Juan, E. Coronado and T. Torres, *Chem. – Eur. J.*, 2013, **19**, 1457; (*b*) Y.-S. Ding, N. F. Chilton, R. E. P. Winpenny and Y.-Z. Zheng, *Angew. Chem., Int. Ed.*, 2016, **55**, 16071; (*c*) Y.-C. Chen, J.-L. Liu, L. Ungur, J. Liu, Q.-W. Li, L.-F. Wang, Z.-P. Ni, L.-F. Chibotaru, X.-M. Chen and M.-L. Tong, *J. Am. Chem. Soc.*, 2016, **138**, 2829; (*d*) S. K. Gupta, T. Rajeshkumar, G. Rajaraman and R. Murugavel, *Chem. Sci.*, 2016, **7**, 5181; (*e*) L. Ungur, J. J. Le Roy, I. Korobkov, M. Murugesu and L. F. Chibotaru, *Angew. Chem., Int. Ed.*, 2014, **53**, 4413; (*f*) J. J. Le Roy, I. Korobkov and M. Murugesu, *Chem. Commun.*, 2014, **50**, 1602.

6 J. Liu, Y.-C. Chen, J.-L. Liu, V. Vieru, L. Ungur, J.-H. Jia, L.-F. Chibotaru, Y.-H. Lan, W. Wernsdorfer, S. Gao, X.-M. Chen and M.-L. Tong, *J. Am. Chem. Soc.*, 2016, **138**, 5441.

7 (*a*) C. A. P. Goodwin, F. Ortu, D. Reta, N. F. Chilton and D. P. Mills, *Nature*, 2017, **548**, 439; (*b*) F.-S. Guo, M. D. Benjamin, Y.-C. Chen, M.-L. Tong, A. Mansikkamäki and A. L. Richard, *Angew. Chem., Int. Ed.*, 2017, **56**, 11445.

8 (*a*) G.-F. Xu, Q.-L. Wang, P. Gamez, Y. Ma, R. Clérac, J. Tang, S.-P. Yan, P. Cheng and D.-Z. Liao, *Chem. Commun.*, 2010, **46**, 1506; (*b*) Y.-N. Guo, G.-F. Xu, W. Wernsdorfer, L. Ungur, Y. Guo, J. Tang, H.-J. Zhang, L. F. Chibotaru and A. K. Powell, *J. Am. Chem. Soc.*, 2011, **133**, 11948; (*c*) P. Zhang, L. Zhang, S.-Y. Lin, S. Xue and J. Tang, *Inorg. Chem.*, 2013, **52**, 4587; (*d*) C. Wang, S.-Y. Lin, J. Wu, S.-W. Yuan and J. Tang, *Dalton Trans.*, 2015, **44**, 4648; (*e*) L. Zhang, J.-L. Jung, P. Zhang, M. Guo, L. Zhao, J. Tang and B. Le Guennic, *Chem. – Eur. J.*, 2016, **22**, 1392.

9 (*a*) C. Y. Chow, H. Bolvin, V. E. Campbell, R. Guillot, J. W. Kampf, W. Wernsdorfer, F. Gendron, J. Autschbach, V. L. Pecoraro and T. Mallah, *Chem. Sci.*, 2015, **6**, 4148; (*b*) F. Habib, P.-H. Lin, J. Long, I. Korobkov, W. Wernsdorfer and M. Murugesu, *J. Am. Chem. Soc.*, 2011, **133**, 8830; (*c*) S. Demir, M. I. Gonzalez, L. E. Darago, W. J. Evans and J. R. Long, *Nat. Commun.*, 2017, **8**, 2144; (*d*) B. S. Dolinar, D. I. Alezandropoulos, K. R. Vignesh, T. James and K. R. Dunbar, *J. Am. Chem. Soc.*, 2018, **140**, 908.

10 J. D. Rinehart, M. Fang, W. J. Evans and J. R. Long, *J. Am. Chem. Soc.*, 2011, **133**, 14236.

11 J. J. Le Roy, L. Ungur, I. Korobkov, L. F. Chibotaru and M. Murugesu, *J. Am. Chem. Soc.*, 2014, **136**, 8003.

12 (*a*) S. Demir, M. Nippe, M. I. Gonzalez and J. R. Long, *Chem. Sci.*, 2014, **5**, 4701; (*b*) S. Demir, J. M. Zadrozny, M. Nippe and J. R. Long, *J. Am. Chem. Soc.*, 2012, **134**, 18546.

13 (*a*) W.-B. Sun, B. Yan, L.-H. Jia, B.-W. Wang, Q. Yang, X. Cheng, H.-F. Li, P. Chen, Z.-M. Wang and S. Gao, *Dalton Trans.*, 2016, **45**, 8790; (*b*) S. Mukherjee, J. Lu, G. Velmurugan, S. Singh, G. Rajaraman, J. Tang and S. K. Ghosh, *Inorg. Chem.*, 2016, **55**, 11283; (*c*) S. Xue, Y.-N. Guo, L. Ungur, J. Tang and L. F. Chibotaru, *Chem. – Eur. J.*, 2015, **21**, 14099; (*d*) B. Joarder, S. Mukherjee, S. Xue, J. Tang and S. K. Ghosh, *Inorg. Chem.*, 2014, **53**, 7554; (*e*) M. Iwan, A. Kula, Z. Rzaczyńska, S. Pikus, D. Flisiuk and M. Gomola, *Chem. Pap.*, 2007, **61**, 376.

14 (*a*) J. J. Baldoví, E. Coronado, A. G. Ariño, C. Gamer, M. G. Marqués and G. M. Espallargas, *Chem. – Eur. J.*, 2014, **20**, 10695; (*b*) K. Liu, H. Li, X. Zhang, W. Shi and P. Cheng, *Inorg. Chem.*, 2015, **54**, 10224; (*c*) S. Zhang, H. Li, E. Duan, Z. Han, L. Li, J. Tang, W. Shi and P. Cheng, *Inorg. Chem.*, 2016, **55**, 1202; (*d*) K. Liu, X. Zhang, X. Meng, W. Shi, P. Cheng and A. K. Powell, *Chem. Soc. Rev.*, 2016, **45**, 2423; (*e*) X. Zhang, N. Xu, W. Shi, B.-W. Wang and P. Cheng, *Inorg. Chem. Front.*, 2018, **5**, 432; (*f*) L. Qin, Y.-Z. Yu, P.-Q. Liao, W. Xue, Z. Zheng, X.-M. Chen and Y.-Z. Zheng, *Adv. Mater.*, 2016, **28**, 10772; (*g*) L. Qin, G.-J. Zhou, Y.-Z. Yu, H. Nojiri, C. Schröder, R. E. P. Winpenny and Y.-Z. Zheng, *J. Am. Chem. Soc.*, 2017, **139**, 16405; (*h*) L. Qin, J. Singleton, W.-P. Chen, H. Nojiri, L. Engelhardt, R. E. P. Winpenny and Y.-Z. Zheng, *Angew. Chem., Int. Ed.*, 2017, **56**, 16571; (*i*) T. Han, Y.-S. Ding and Y.-Z. Zheng, *Struct. Bonding*, Springer, Berlin, 2016, vol. 173, p. 209.

15 (*a*) X. Zhang, V. Vieru, X. Feng, J.-L. Liu, Z. Zhang, B. Na, W. Shi, B.-W. Wang, A. K. Powell, L. F. Chibotaru, S. Gao, P. Cheng and J. R. Long, *Angew. Chem., Int. Ed.*, 2015, **54**, 9861; (*b*) J.-L. Liu, J.-Y. Wu, G.-Z. Huang, Y.-C. Chen, J.-H. Jia, L. Ungur, L. F. Chibotaru, X.-M. Chen and M.-L. Tong, *Sci. Rep.*, 2015, **5**, 16621; (*c*) M. Ren, D. Pinkowicz, M. Yoon, K. Kim, L.-M. Zheng, B. K. Breedlove and M. Yamashita, *Inorg. Chem.*, 2013, **52**, 8342; (*d*) J. Liu, X.-P. Zhang, T. Wu, B.-B. Ma, T.-W. Wang, C.-H. Li, Y.-Z. Li and X.-Z. You, *Inorg. Chem.*, 2012, **51**, 8649; (*e*) Y. Zhu, F. Luo, M. Luo, X. Feng, S. R. Batten, G. Sun, S. Liu and W. Xu, *Dalton Trans.*, 2013, **42**, 8545; (*f*) G. Redler, C. Lampropoulos, S. Datta, C. Koo, T. C. Stamatatos, N. E. Chakov, G. Christou and S. Hill,

*Phys. Rev. B: Condens. Matter Mater. Phys.*, 2009, **80**, 094408.

16 (*a*) J.-L. Du, G. R. Eaton and S. S. Eaton, *J. Magn. Reson., Ser. A*, 1995, **2**, 213; (*b*) J. M. Zadrozny, J. Niklas, O. G. Poluektov and D. E. Freedman, *ACS Cent. Sci.*, 2015, **1**, 488.

17 H.-R. Tu, W.-B. Sun, H.-F. Li, P. Chen, Y.-M. Tian, W.-Y. Zhang, Y.-Q. Zhang and P.-F. Yan, *Inorg. Chem. Front.*, 2017, **4**, 499.

18 (*a*) S. Alvarez, P. Alemany, D. Casanova, J. Cirera, M. Llunell and D. Avnir, *Coord. Chem. Rev.*, 2005, **249**, 1693; (*b*) M. Llunell, D. Casanova, J. Cirera, P. Alemany and S. Alvarez, *SHAPE, v2.1*, University of Barcelona and The Hebrew University of Jerusalem, Barcelona and Jerusalem, 2013.

19 (*a*) M. Ren, S.-S. Bao, N. Hoshino, T. Akutagawa, B.-W. Wang, Y.-C. Ding, S.-Q. Wei and L.-M. Zheng, *Chem. – Eur. J.*, 2013, **19**, 9619; (*b*) J. Wu, J. Jung, P. Zhang, H. Zhang, J. Tang and B. L. Guennic, *Chem. Sci.*, 2016, **7**, 3632.

20 G. Karlström, R. Lindh, P.-Å. Malmqvist, B. O. Roos, U. Ryde, V. Veryazov, P.-O. Widmark, M. Cossi, B. Schimmelpfennig, P. Neograd and L. Seijo, *Comput. Mater. Sci.*, 2003, **28**, 222.

21 M. E. Lines, *J. Chem. Phys.*, 1971, **55**, 2977.

22 (*a*) K. S. Cole and R. H. J. Cole, *J. Chem. Phys.*, 1941, **9**, 341; (*b*) S. M. J. Aubin, Z. Sun, L. Pardi, J. Krzystek, K. Folting, L.-C. Brunel, A. L. Rheingold, G. Christou and D. N. Hendrickson, *Inorg. Chem.*, 1999, **38**, 5329.

23 D. Gatteschi, R. Sessoli and J. Villain, *Molecular Nanomagnets*, Oxford University Press, New York, 2006 and references therein.

24 (*a*) P.-H. Lin, T. J. Burchell, L. Ungur, L. F. Chibotaru, W. Wernsdorfer and M. Murugesu, *Angew. Chem., Int. Ed.*, 2009, **48**, 9489; (*b*) I. J. Hewitt, Y. Lan, C. E. Anson, J. Luzon, R. Sessoli and A. K. Powell, *Chem. Commun.*, 2009, 6765.

25 J. Tang, I. Hewitt, N. T. Madhu, G. Chastanet, W. Wernsdorfer, C. E. Anson, C. Benelli, R. Sessoli and A. K. Powell, *Angew. Chem., Int. Ed.*, 2006, **45**, 1729.

26 P.-H. Lin, T. J. Burchell, R. Clérac and M. Murugesu, *Angew. Chem., Int. Ed.*, 2008, **47**, 8848.

27 S.-D. Jiang, B.-W. Wang, G. Su, Z.-M. Wang and S. Gao, *Angew. Chem.*, 2010, **122**, 7610.

28 W. Wernsdorfer, *Supercond. Sci. Technol.*, 2009, **22**, 064013.

29 (*a*) T. Han, J.-D. Leng, Y.-S. Ding, Y. Wang, Z. Zheng and Y.-Z. Zheng, *Dalton Trans.*, 2015, **44**, 13480; (*b*) Y. Wang, T. Han, Y.-S. Ding, Z. Zheng and Y.-Z. Zheng, *Dalton Trans.*, 2016, **45**, 1130.

30 D. Pinkowicz, H. I. Southerland, C. Avendaño, A. Prosvirin, C. Sanders, W. Wernsdorfer, K. S. Pedersen, J. Dreiser, R. Clérac, J. Nehrkorn, G. G. Simeoni, A. Schnegg, K. Holldack and K. R. Dunbar, *J. Am. Chem. Soc.*, 2015, **137**, 14406.

31 (*a*) J.-L. Liu, K. Yuan, J. D. Leng, L. Ungur, W. Wernsdorfer, F. S. Guo, L. F. Chibotaru and M.-L. Tong, *Inorg. Chem.*, 2012, **51**, 8538; (*b*) E. Colacio, J. Ruiz, E. Ruiz, E. Cremades, J. Krzystek, S. Carretta, J. Cano, T. Guidi, W. Wernsdorfer, S. Crretta and E. K. Brechin, *Angew. Chem., Int. Ed.*, 2013, **52**, 9130; (*c*) W.-B. Sun, B. Yan, Y.-Q. Zhang, B.-W. Wang, Z.-M. Wang, J.-H. Jia and S. Gao, *Inorg. Chem. Front.*, 2014, **1**, 503.

32 (*a*) J. Luzon, K. Bernot, I. J. Hewitt, C. E. Anson, A. K. Powell and R. Sessoli, *Phys. Rev. Lett.*, 2008, **100**, 247205; (*b*) R. A. Layfield, J. J. W. McDouall, S. A. Sulway, F. Tuna, D. Collison and R. E. P. Winpenny, *Chem. – Eng. J.*, 2010, **16**, 4442.

33 X. Yi, K. Bernt, F. Pointillart, G. Poneti, G. Calvez, C. Daiguebonne, O. Guillou and R. Sessoli, *Chem. – Eur. J.*, 2012, **18**, 11379.

34 R. Bagai, W. Wernsdorfer, K. A. Abboud and G. Christou, *J. Am. Chem. Soc.*, 2007, **129**, 12918.

35 J. S. Costa, N. A. Bandeira, B. Le Guennic, V. Robert, P. Gamez, G. Chastanet, L. Ortiz-Frade and L. Gasque, *Inorg. Chem.*, 2011, **50**, 5696.

36 (*a*) G. Cosquer, F. Pointillart, S. Golhen, O. Cador and L. Ouahab, *Chem. – Eur. J.*, 2013, **19**, 7895; (*b*) E. Bartolomé, J. Bartolomé, S. Melnic, D. Prodius, S. Shova, A. Arauzo, J. Luzón, F. Luis and C. Turta, *Dalton Trans.*, 2013, **42**, 10153; (*c*) S. Zhang, H. Ke, L. Sun, X. Li, Q. Shi, G. Xie, Q. Wei, D. Yang, W. Wang and S. Chen, *Inorg. Chem.*, 2016, **55**, 3865.

37 F. Moro, D. P. Mills, S. T. Liddle and J. van Slageren, *Angew. Chem.*, 2013, **125**, 3514.

38 M. Murugesu, *Nat. Chem.*, 2012, **4**, 347.

39 (*a*) L. F. Chibotaru, L. Ungur and A. Soncini, *Angew. Chem., Int. Ed.*, 2008, **120**, 4194; (*b*) L. Ungur, W. Van den Heuvel and L. F. Chibotaru, *New J. Chem.*, 2009, **33**, 1224; (*c*) L. F. Chibotaru, L. Ungur, C. Aronica, H. Elmoll, G. Pilet and D. Luneau, *J. Am. Chem. Soc.*, 2008, **130**, 12445.

40 (*a*) G. M. Sheldrick, *Acta Crystallogr., Sect. C: Struct. Chem.*, 2015, **71**, 3; (*b*) O. V. Dolomanov, L. J. Bourhis, R. J. Gildea, J. A. K. Howard and H. Puschmann, *J. Appl. Crystallogr.*, 2009, **42**, 339; (*c*) L. Farrugia, *J. Appl. Crystallogr.*, 2012, **45**, 849.

 